Nuclear Materials and Energy 34 (2023) 101348

Contents lists available at ScienceDirect

Nuclear Materials and Energy

journal homepage: www.elsevier.com/locate/nme

Hydrogen isotope exchange experiments in high entropy alloy WMoTaNbV

T. Vuoriheimo [a,*], A. Liski [a], P. Jalkanen [a], T. Ahlgren [a], K. Mizohata [a], K. Heinola [b], Y. Zayachuk [c], K.–K. Tseng [d], C.–W. Tsai [d,e], J.–W. Yeh [d,e], F. Tuomisto [a]

[a] Department of Physics, University of Helsinki, P.O. Box 43, 00014 Helsinki, Finland
[b] International Atomic Energy Agency IAEA, Vienna International Centre, P.O. Box 100, 1400 Vienna, Austria
[c] UK Atomic Energy Authority, Culham Science Centre, Abingdon OX14 3DB, United Kingdom
[d] Department of Materials Science and Engineering, National Tsing Hua University, Hsinchu 30013, Taiwan
[e] High Entropy Materials Center, National Tsing Hua University, Hsinchu 30013, Taiwan

ARTICLE INFO

Keywords:
Deuterium
High entropy alloy
Isotope exchange
Fuel retention

ABSTRACT

Plasma–facing components in future fusion reactors must endure high temperatures as well as high fluxes and fluences of high energy particles. Currently tungsten has been chosen as the primary plasma-facing material due to its good thermal conductivity, low erosion rate and low fuel retention. Materials with even better properties are still being investigated to be used in reactor regions with demanding plasma conditions. High entropy alloys (HEA) are a new class of metallic alloys and their exploitation in fusion applications has not been widely studied. In this work, the hydrogen isotope exchange effect in an equiatomic HEA containing W, Mo, Ta, Nb, and V was studied. Deuterium was implanted into HEA samples with 30 keV/D energy and the HEA and reference samples were annealed in H_2 atmosphere and in vacuum at various temperatures up to 400 °C, respectively. The near-surface D concentration profiles were measured with ERDA and the isotope exchange was observed to remove over 90 % of the trapped deuterium from the implantation region at temperatures above 200 °C. TDS was used to measure retention deeper in the bulk in which the reduction of trapped deuterium was significantly lower. High total retention of H was found in the bulk after H_2 atmosphere annealing which indicates permeation and deep trapping of H in the material.

1. Introduction

In fusion reactors, plasma-facing components (PFCs) and structural materials need to withstand high doses of radiation and particles. Tungsten (W) is currently planned as PFC material for ITER (divertor) and European DEMO (divertor and main chamber) whereas reduced-activation ferritic materials (RAFM) are favored to be used in the structural components. These RAFM-based components are mostly influenced by neutron irradiation-induced damage, whereas W, being installed close to the plasma, may encounter problems when exposed directly to high flux and high energy particles. Hydrogen isotopes, alpha particles and neutrons cause irradiation-induced defects which can modify the mechanical properties of W. The defects also increase fuel retention by forming trap sites for hydrogen isotopes. The corresponding fuel retention must be controlled in order to minimize the in-vessel inventory of hydrogen radioactive isotope tritium (T).

To improve the radiation tolerance of reactor components, new materials need to be fabricated and tested for fusion applicability. High entropy alloys (HEAs) are novel materials that contain five or more elements in equiatomic proportions. HEAs combine different beneficial properties of these elements as well as create new properties due to mixing of the elements. For example, due to low mobility of defects and interstitials, HEAs form fewer defect clusters than W when exposed to high energy particles [1,2] and have enhanced mechanical properties such as increased irradiation resistance on hardness [3]. High radiation tolerance can be utilized in high flux areas of a fusion reactor such as divertors. A recent review discusses many properties of HEAs for nuclear applications, such as activation issues, thermal conductivity, and defect formation, and found them promising due to their tunability for different conditions [4]. More research is needed to understand better the usability and benefits of different HEA materials for fusion. In this study we are focusing on HEA consisting of W, Mo, Ta, Nb, and V and its application under PFC conditions. Hydrogen isotope retention properties on this material have been studied in another paper [5].

Conventionally trapped hydrogen isotopes are removed from PFCs by annealing the material at high temperatures. An efficient method to

* Corresponding author.
E-mail address: tomi.vuoriheimo@helsinki.fi (T. Vuoriheimo).

https://doi.org/10.1016/j.nme.2022.101348
Received 20 October 2022; Received in revised form 5 December 2022; Accepted 19 December 2022
Available online 20 December 2022

remove trapped T from the PFCs is by using isotope exchange effect in which a lighter isotope of hydrogen replaces trapped T atoms. By using isotope exchange the temperatures required to remove trapped T can be significantly lowered which reduces the energy consumption required for the annealing. Hydrogen isotope exchange has been studied previously in W by implanting lighter isotope protium (H) [6–9] and by annealing the material in hydrogen isotope gas [10–13]. The effect has also been studied by reversing the situation by replacing lighter isotopes with heavier isotopes [11,14] and by modelling [15–17]. The results are promising and show that isotope exchange may increase the efficiency of tritium removal from PFCs in the future. However, the previous studies have all focused on W. In this work we study how the isotope exchange functions with the HEA material. To avoid safety problems arising from radioactive materials, we used deuterium (D) as a substitute for T.

2. Materials and methods

2.1. Sample preparation

HEA samples consisting of W, Mo, Ta, Nb, and V were prepared by High Entropy Materials Center of National Tsing Hua University by vacuum arc melting with details of the preparation given in Ref. [18]. Mechanical properties and microstructure of the material are reported in Ref. [19]. The samples were 5 × 5 mm^2 in size and 1 mm thick. The samples were polished mechanically using diamond suspension with different grain sizes down to 50 nm. After polishing, the samples were pre–annealed in a vacuum of 10^{-7} mbar at 1000 °C for two hours to reduce the amount of impurities, including protium, and defects.

2.2. Deuterium implantations

D implantations were made using a 500 kV implanter at University of Helsinki. D was implanted as D_2^+ ions using 30 keV/D implantation energy and fluence of the implantation was 5.8 × 10^{16} D/cm^2. The ion energy and fluence were chosen based on a previous study on W [10] for easy comparison of materials. Ion beam was raster scanned over the samples to ensure homogeneous implantation profile. The flux of the ion beam was about 1 × 10^{13} D/cm^2s. The implantation was done at room temperature (RT).

2.3. Sample annealing

Implanted samples were annealed for 4 h in a quartz tube at RT, 100 °C, 200 °C, 300 °C, and 400 °C. Samples for isotope exchange were annealed in 1 bar H_2 atmosphere and reference samples in a vacuum of about 10^{-6} mbar. A constant gas flow was kept during the H_2 atmosphere annealing.

2.4. Elastic recoil detection analysis

The D concentration near the sample surface up to 400 nm was measured using Elastic Recoil Detection Analysis (ERDA). 24 MeV $^{28}Si^{5+}$ ions were used in the measurement. Incident angle was 30° and exit angle was 15° which made the total scattering angle 45°. A Havar foil with 4.0 μm thickness was placed in front of the detector to prevent the recoiled ion beam and other heavier ions from reaching the detector. The detector had a nominal energy resolution of 15 keV and it was placed 50 mm from the sample with a 2 × 7 mm^2 collimator. Secondary electron emission was suppressed using a negatively charged net around the sample holder. The ion, its energy, and the angles were chosen to maximize depth resolution around the implanted depth and to prevent H and D signals from overlapping. D concentrations were calculated using D-implanted Si reference samples and normalized using ion beam profilometer data.

2.5. Thermal desorption spectrometry

To confirm the total amount of retained D, Thermal Desorption Spectrometry (TDS) was performed to the samples subsequently to the ERDA measurements. The TDS analyses were performed at Culham Centre for Fusion Energy using Hiden Analytical ltd Type 640,100 TPD Workstation. Details of the measurement system are explained in Ref. [20]. Samples were annealed from room temperature to 850 °C at a constant rate of 5 °C/min or 10 °C/min depending on the sample and kept at 850 °C for two hours. The annealing was performed on a molybdenum stage in vacuum of 3 × 10^{-9} mbar. The samples were placed on a heater stage and heated from the backside. The desorbed molecules were measured by a line-of-sight Quadrupole Mass Spectrometer (QMS). Mass signals of 2, 3, and 4, corresponding to H_2, HD and D_2 molecules respectively, were measured to obtain total amount of desorbed H and D, which were calculated as $H_{atomic} = 2 \times H_2$ and $D_{atomic} = HD + 2 \times D_2$. The effect of H_3 molecule on mass 3 signal was taken into account in the analysis. Signals were calibrated using calibrated leaks for H_2 and D_2, with calibration factor for HD calculated as average between the two. Signals corresponding to 18 (H_2O), 19 (HDO), 20 (D_2O), 28 (N_2), 32 (O_2), and 44 (CO_2) were also monitored but not quantified for possible contaminants desorbing from the samples.

3. Results and discussion

3.2. Near-surface concentrations

D and H areal densities were measured by ERDA and analyzed up to depth of 300 nm. Simulations done by SRIM code [21] estimate that 95 % of implanted D ions are stopped within the first 300 nm as shown in Fig. 1. The implantation–induced defects are all formed within the first 300 nm. Therefore the isotope exchange effect happening in the near-surface implantation-induced traps can be observed by ERDA.

The absolute values of the areal density are shown on Fig. 2 (a) for both H and D and the relative amount of D compared to the as-implanted sample is shown on Fig. 2 (b). It is worth noting that only about 20 % of the implanted D has been trapped within the first 300 nm while most of the D has diffused deeper into the sample. Error bars on Fig. 2 are based on the square roots of ERDA counts integrated over the analyzed depth. The estimate for the depth profiles based on the particle energies is presented on Fig. 3 (a). The shape of the depth profiles changed slightly as the near-surface D concentration decreased during the ERDA measurements as seen on Fig. 3 (b). This suggests that D is detrapping from the implantation-induced traps and getting trapped again deeper in the sample.

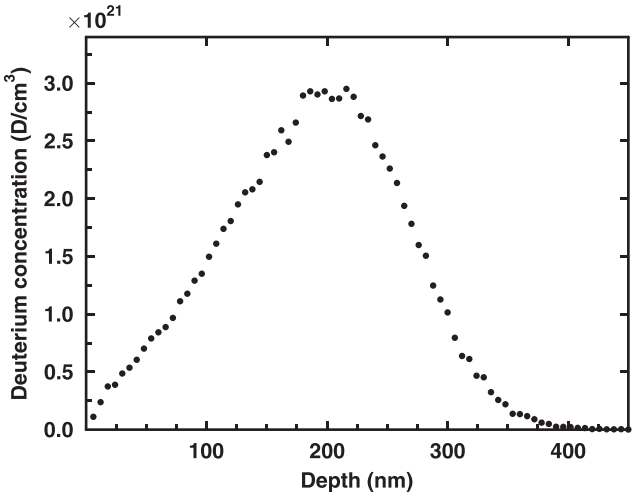

Fig. 1. Implanted ion depth distribution simulated by SRIM.

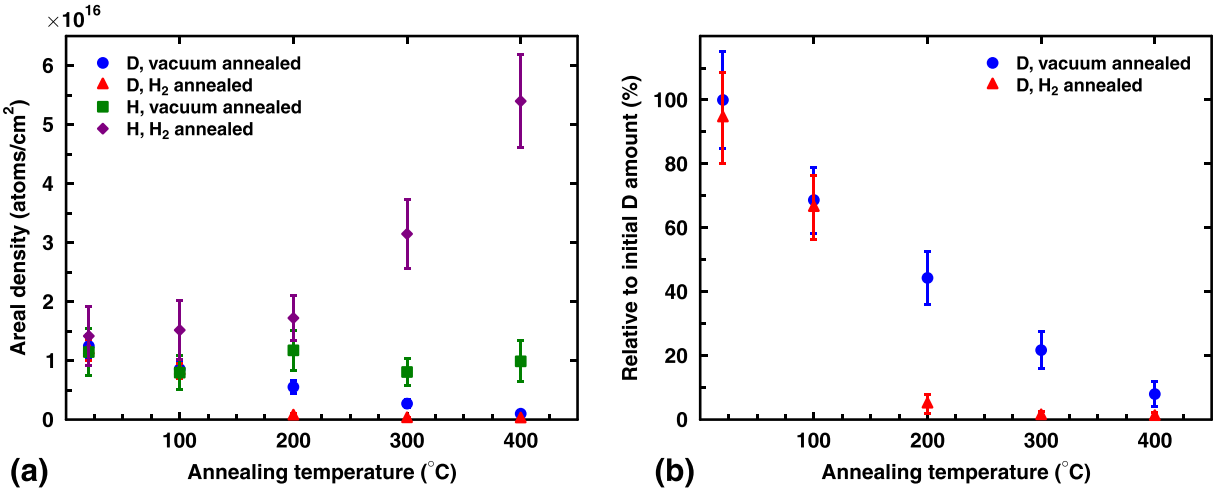

Fig. 2. Results from ERDA measurements after annealing the samples at various temperatures. (a) Areal density of H and D. (b) Relative change of D areal density in the sample in comparison to unannealed sample.

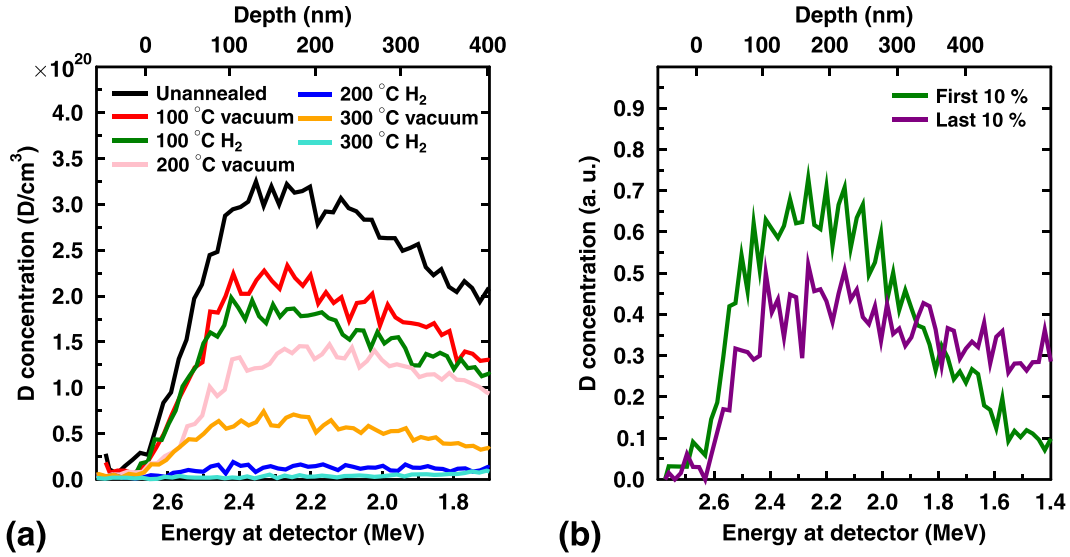

Fig. 3. Energy profiles of ERDA measurements with concentrations corrected using cross sections and estimates for corresponding depths. (a) Profiles for D in various samples. Samples annealed at 400 °C contained very little D. (b) First 10 % and last 10 % of data of the unannealed sample measurement. The change in profile during measurement suggests D moving deeper into the sample during the measurement.

On Fig. 2 (b) there is a clear trend of decreasing D concentration as the annealing temperatures are increased. The implantation–induced trap sites are releasing trapped D already at 100 °C as the amount of D has decreased similarly with both vacuum and H_2 atmosphere annealing. Vacuum annealed samples have a steady decrease up to the maximum temperature of 400 °C at which there is 8 % of D remaining. H_2 annealed samples, however, show a significant reduction in D amounts at and above 200 °C. The amount of D decreases down to 5 % at 200 °C and is furthermore reduced down to 1 % at higher temperatures. From this we can see that annealing in H_2 atmosphere has a significant effect in reduction of D retention in the near–surface depth where the implantation–induced damage is formed. Isotope exchange effect is efficiently removing the trapped D from the irradiation–induced trap sites compared to annealing in vacuum at 200 °C and 300 °C.

Areal densities of H are higher at all temperatures with the H_2 annealed samples than with vacuum annealed samples as shown on Fig. 2 (a). This increase is significantly increased at 300 °C and above. From these amounts it is apparent that H is not only replacing D in the traps but also being trapped to other trap sites in the material as the increase in H amount is much higher than the decrease in D amount. In similar experiments with W the amount of desorbed D is much higher than absorbed H, and H trapping in W is therefore limited by the amount of implantation–induced trap sites [10,11].

3.2. Bulk concentrations

As only a small portion of the implanted D is trapped near the surface, the D amount in bulk was measured by TDS to investigate whether the isotope exchange effect is affecting D trapped deeper in the HEA. Results of the measurements are shown on Fig. 4. The error bars on Fig. 4 are calculated from the uncertainty of implanted area due to sample holder clips covering part of the samples during implantations. We can see that the significant reduction in D amounts seen on Fig. 2 is not happening in bulk in either vacuum or H_2 atmosphere. In the samples annealed in vacuum the amount of D is not seen to decrease, and in the samples annealed in H_2 atmosphere there is a 40 % decrease at 300 °C, in contrast to 99 % decrease in the near-surface region. This means that D has been replaced in the near-surface implantation-induced traps but

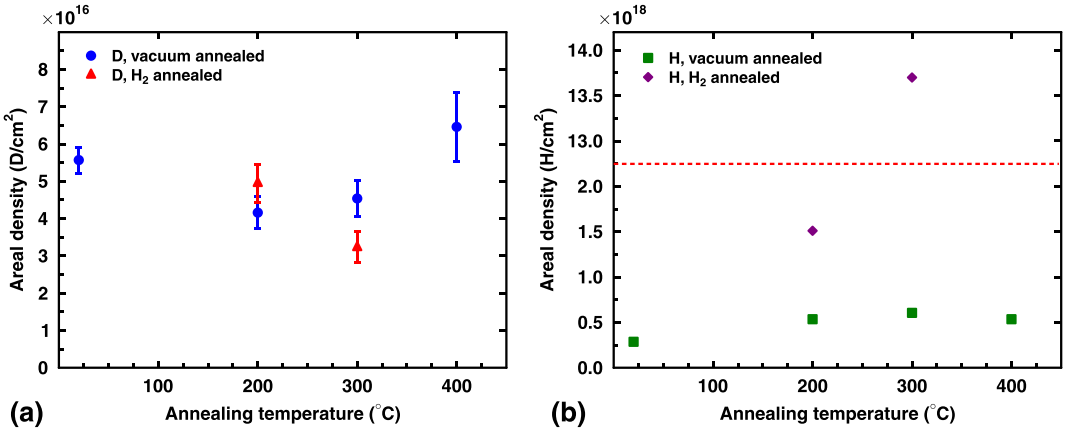

Fig. 4. Total areal densities after annealing the samples at various temperatures measured by TDS. (a) Areal density of D. (b) Areal density of H from the same samples. The y axis is broken at the red line as one sample contains much more H than others. (For interpretation of the references to colour in this figure legend, the reader is referred to the web version of this article.)

deeper in the bulk most of the trapped D still remains. The TDS results on Fig. 5 show that D is not desorbing from the sample below 400 °C and temperatures over 600 °C are needed to remove the remaining D from the sample. Temperatures below 600 °C are sufficient to desorb almost all D from W [22].

By using the total amount of H desorbed from the samples and the annealing time in H_2 atmosphere, we can estimate that the H flux into the bulk during the four hour annealing on average is 7×10^{13} H/(cm_2s) at 200 °C and 9×10^{14} H/(cm_2s) at 300 °C. These fluxes are much higher than in W in which the surface-to-bulk atomic fluxes are estimated to be 10^{11} H/(cm_2s) and 10^{14}H/(cm_2s) at 200 °C and 300 °C, respectively [10]. Because the HEA has higher surface-to-bulk H flux at 200 °C than W, the isotope exchange effect is taking place in the implantation–induced trap sites much more efficiently. W requires temperatures above 300 °C or longer annealing times to obtain high enough excess solute H concentrations in the bulk to achieve efficient isotope exchange [10,11]. In the HEA bulk, the trapped D does not get replaced as efficiently even when the amount of excess H is increased.

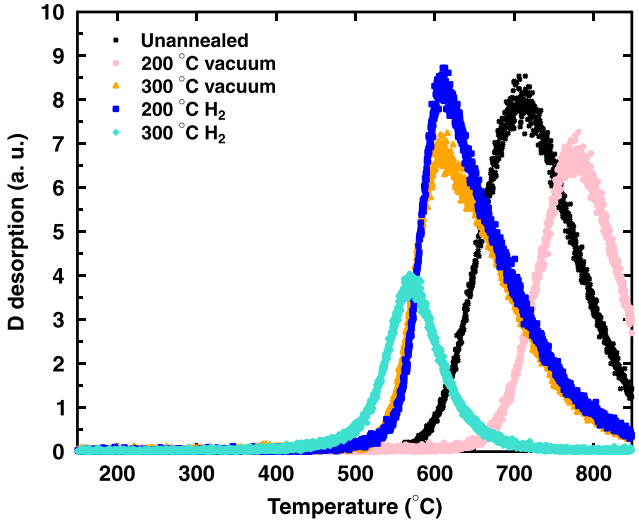

Fig. 5. D desorption results of TDS measurements normalized to total desorption per kelvin to account for different heating rates. The shift to lower desorption temperature with 300 °C sample is caused by 5 °C/min heating rate as opposed to other samples having 10 °C/min heating rate. The shift to higher temperatures on unannealed sample and 200 °C vacuum annealed sample is likely an experimental error but it is not affecting the total desorption results.

4. Conclusions

Our experiments show a significant reduction of D retention in the near-surface trap sites with isotope exchange effect in the HEA material. Temperature required to remove over 90 % of trapped D from the first 400 nm below the surface is much lower than has been observed with W when using isotope exchange. Together with the higher radiation tolerance reported for HEAs, the results are promising in the near–surface regions.

Results from the bulk, however, show that the D has not been removed as efficiently deeper in the material. H_2 atmosphere annealing decreases the amount of retained D in the bulk but not as much as in the near-surface region. It is unclear whether the efficiency is limited by the amount of H diffused deeper in the bulk or by trap sites not exchanging the isotopes as efficiently as in the implantation–induced defects. In vacuum annealing the amount of retained D is observed to decrease in the near–surface region at 400 °C by over 90 %, but no significant reduction is happening in the bulk. The near–surface trap sites can be assumed to release the trapped D which is subsequently trapped again to the intrinsic trap sites in the bulk. The origin of these trap sites is not known and requires further research. Possible options are for example dislocation-type defects, grain boundaries, impurities, and compounds with the sample elements.

Saturation limit of H retention is not seen in our results for either near-surface or bulk. The total retention of H after annealing in H_2 atmosphere at higher temperatures is very high and temperatures over 600 °C are needed to remove hydrogen isotopes from the material. The permeation of H into the bulk is high which can cause serious problems with for example coolant contamination. These findings are highly worrying when considering HEAs as possible PFC materials. Amount of intrinsic trap sites need to be reduced either by changing the composition of the HEA or by different manufacturing methods depending on the trap. Research on hydrogen retention including trapping energies in this HEA material is presented in [5] and therefore not addressed in this paper. More in-depth details of retention mechanisms in HEA are a part of our future work.

CRediT authorship contribution statement

T. Vuoriheimo: Investigation, Formal analysis, Software, Data curation, Visualization, Writing – original draft. **A. Liski:** Resources. **P. Jalkanen:** Resources. **T. Ahlgren:** Conceptualization, Methodology, Project administration. **K. Mizohata:** Methodology, Software. **K. Heinola:** Writing – review & editing, Supervision. **Y. Zayachuk:** Investigation, Formal analysis. **K.–K. Tseng:** Resources. **C.–W. Tsai:** Resources. **J.–W. Yeh:** Resources. **F. Tuomisto:** Supervision.

Declaration of Competing Interest

The authors declare that they have no known competing financial interests or personal relationships that could have appeared to influence the work reported in this paper.

Data availability

Data will be made available on request.

Acknowledgements

This work has been carried out within the framework of the EUROfusion Consortium, funded by the European Union via the Euratom Research and Training Programme (Grant Agreement No 101052200 — EUROfusion). Views and opinions expressed are however those of the author(s) only and do not necessarily reflect those of the European Union or the European Commission. Neither the European Union nor the European Commission can be held responsible for them.

This work was financially supported by the "High Entropy Materials Center" from The Featured Areas Research Center Program within the framework of the Higher Education Sprout Project by the Ministry of Education (MOE) and from the Project NSTC 111-2634-F-007-008 and NSTC111-2224-E-007-003 by National Science and Technology Council (NSTC) in Taiwan.

References

[1] O. El-Atwani, N. Li, M. Li, A. Devaraj, J.K.S. Baldwin, M.M. Schneider, D. Sobieraj, J.S. Wróbel, D. Nguyen-Manh, S.A. Maloy, E. Martinez, Outstanding radiation resistance of tungsten-based high-entropy alloys, Sci. Adv. 5 (2019) eaav2002, https://doi.org/10.1126/sciadv.aav2002.

[2] F. Granberg, K. Nordlund, M.W. Ullah, K. Jin, C. Lu, H. Bei, L.M. Wang, F. Djurabekova, W.J. Weber, Y. Zhang, Mechanism of Radiation Damage Reduction in Equiatomic Multicomponent Single Phase Alloys, Phys. Rev. Lett. 116 (2016), 135504, https://doi.org/10.1103/PhysRevLett.116.135504.

[3] M. Sadeghilaridjani, A. Ayyagari, S. Muskeri, V. Hasannaeimi, R. Salloom, W.-Y. Chen, S. Mukherjee, Ion irradiation response and mechanical behavior of reduced activity high entropy alloy, J. Nucl. Mater. 529 (2020), 151955, https://doi.org/10.1016/j.jnucmat.2019.151955.

[4] E.J. Pickering, A.W. Carruthers, P.J. Barron, S.C. Middleburgh, D.E.J. Armstrong, A.S. Gandy, High-Entropy Alloys for Advanced Nuclear Applications, Entropy 23 (2021), https://doi.org/10.3390/e23010098.

[5] A. Liski, T. Vuoriheimo, P. Jalkanen, K. Mizohata, E. Lu, J. Likonen, J. Heino, K. Heinola, Y. Zayachuk, A. Widdowson, K.-K. Tseng, C.-W. Tsai, J.-W. Yeh, F. Tuomisto, T. Ahlgren, Irradiation Damage Independent Deuterium Retention in WMoTaNbV, Materials (Basel). 15 (2022), https://doi.org/10.3390/ma15207296.

[6] J. Roth, T. Schwarz-Selinger, V.K. Alimov, E. Markina, Hydrogen isotope exchange in tungsten: Discussion as removal method for tritium, J. Nucl. Mater. 432 (2013) 341–347, https://doi.org/10.1016/j.jnucmat.2012.08.004.

[7] V.K. Alimov, B. Tyburska-Püschel, M.H.J. 't Hoen, J. Roth, Y. Hatano, K. Isobe, M. Matsuyama, T. Yamanishi, Hydrogen isotope exchange in tungsten irradiated sequentially with low-energy deuterium and protium ions, Phys. Scr. T145 (2011) 14037. 10.1088/0031-8949/2011/t145/014037.

[8] N.P. Bobyr, V.K. Alimov, B.I. Khripunov, A.V. Spitsyn, M. Mayer, Y. Hatano, A. V. Golubeva, V.B. Petrov, Influence of helium on hydrogen isotope exchange in tungsten at sequential exposures to deuterium and helium–protium plasmas, J. Nucl. Mater. 463 (2015) 1122–1124, https://doi.org/10.1016/j.jnucmat.2014.12.022.

[9] J.L. Barton, Y.Q. Wang, T. Schwarz-Selinger, R.P. Doerner, G.R. Tynan, Isotope exchange experiments in tungsten with sequential deuterium and protium plasmas in PISCES, J. Nucl. Mater. 438 (2013), https://doi.org/10.1016/j.jnucmat.2013.01.261.

[10] T. Ahlgren, P. Jalkanen, K. Mizohata, V. Tuboltsev, J. Räisänen, K. Heinola, P. Tikkanen, Hydrogen isotope exchange in tungsten during annealing in hydrogen atmosphere, Nucl. Fusion. 59 (2019) 26016, https://doi.org/10.1088/1741-4326/aaf6c9.

[11] T. Vuoriheimo, P. Jalkanen, A. Liski, K. Mizohata, T. Ahlgren, K. Heinola, J. Raïsänen, Hydrogen isotope exchange mechanism in tungsten studied by ERDA, Phys. Scr. 2020 (2020), 014056, https://doi.org/10.1088/1402-4896/ab57ad.

[12] Y. Nobuta, Y. Hatano, S.E. Lee, M. Nakayama, Hydrogen isotope exchange in tungsten during heating in hydrogen isotope gas atmosphere, Fusion Eng. Des. 157 (2020), 111703, https://doi.org/10.1016/J.FUSENGDES.2020.111703.

[13] Y. Nobuta, Y. Hatano, Y. Torikai, M. Nakayama, Effects of baking in deuterium atmosphere on tritium removal from tungsten, Fusion Eng. Des. 136 (2018) 674–677, https://doi.org/10.1016/J.FUSENGDES.2018.03.054.

[14] S. Markelj, A. Založnik, T. Schwarz-Selinger, O.V. Ogorodnikova, P. Vavpetič, P. Pelicon, I. Čadež, In situ NRA study of hydrogen isotope exchange in self-ion damaged tungsten exposed to neutral atoms, J. Nucl. Mater. 469 (2016) 133–144, https://doi.org/10.1016/j.jnucmat.2015.11.039.

[15] J.L. Barton, Y.Q. Wang, R.P. Doerner, G.R. Tynan, Development of an analytical diffusion model for modeling hydrogen isotope exchange, J. Nucl. Mater. 463 (2015) 1129–1133, https://doi.org/10.1016/j.jnucmat.2014.12.116.

[16] O. Lindblom, T. Ahlgren, K. Heinola, Molecular dynamics simulations of hydrogen isotope exchange in tungsten vacancies, Nucl. Mater. Energy. 29 (2021), 101099, https://doi.org/10.1016/j.nme.2021.101099.

[17] E.A. Hodille, M. Payet, V. Marascu, S. Peillon, J. Mougenot, Y. Ferro, R. Delaporte-Mathurin, F. Leblond, E. Bernard, C. Grisolia, Modelling tritium adsorption and desorption from tungsten dust particles with a surface kinetic model, Nucl. Fusion. 61 (2021), 086030, https://doi.org/10.1088/1741-4326/ac0f37.

[18] K.K. Tseng, C.C. Juan, S. Tso, H.C. Chen, C.W. Tsai, J.W. Yeh, Effects of Mo, Nb, Ta, Ti, and Zr on mechanical properties of equiatomic Hf-Mo-Nb-Ta-Ti-Zr alloys, Entropy 21 (2019), https://doi.org/10.3390/e21010015.

[19] O.N. Senkov, G.B. Wilks, J.M. Scott, D.B. Miracle, Mechanical properties of Nb25Mo25Ta25W25 and V20Nb20Mo20Ta20W20 refractory high entropy alloys, Intermetallics. 19 (2011) 698–706, https://doi.org/10.1016/j.intermet.2011.01.004.

[20] A. Baron-Wiechec, K. Heinola, J. Likonen, E. Alves, N. Catarino, J.P. Coad, V. Corregidor, I. Jepu, G.F. Matthews, A. Widdowson, Thermal desorption spectrometry of beryllium plasma facing tiles exposed in the JET tokamak, Fusion Eng. Des. 133 (2018) 135–141, https://doi.org/10.1016/J.FUSENGDES.2018.05.075.

[21] J. Ziegler, SRIM, (2013). http://www.srim.org (accessed February 15, 2022).

[22] T. Ahlgren, K. Heinola, E. Vainonen-Ahlgren, J. Likonen, J. Keinonen, Quantification of deuterium irradiation induced defect concentrations in tungsten, Nucl. Instruments Methods Phys. Res. Sect. B Beam Interact. Mater. Atoms. 249 (2006) 436–439, https://doi.org/10.1016/J.NIMB.2006.03.025.